JOURNAL OF COMPUTATIONAL PHYSICS 101, 151–164 (1992)

On Multigrid Solution of High-Reynolds Incompressible Entering Flows*

A. BRANDT

Department of Applied Mathematics, The Weizmann Institute of Science, Rehovot 76100, Israel

AND

I. YAVNEH

Center for Nonlinear Studies and T-7, Los Alamos National Laboratory, Los Alamos, New Mexico 87545
and Department of Applied Mathematics, The Weizmann Institute of Science, Rehovot 76100, Israel

Received October 16, 1990; revised July 19, 1991

An approach is presented for effectively separating the solution process of the elliptic component of high-Reynolds incompressible steady entering flow, for which classical multigrid techniques are well-suited, from that of the non-elliptic part, for which other methods are more effective. It is shown by analysis and numerical calculations that such an approach is very effective in terms of asymptotic convergence as well as reduction of errors well below discretization level in a 1FMG algorithm.

1. INTRODUCTION

Multigrid methods for the numerical solution of elliptic partial differential equations have been studied extensively. Although research continues, there is already much evidence to indicate that the solution of general elliptic systems with general boundary conditions can be obtained in just a few *minimal* work units, which are defined as the number of operations required in the *simplest* discretization of the system on the finest grid. However, attempts to apply these same techniques to systems which have non-elliptic components, such as steady state incompressible flows at the inviscid limit, have met with more limited success. Although such methods are usually much more efficient than comparable single-grid methods, the goal of solution in just a few *minimal* work units has not been attained. Indeed, many reported solvers require hundreds of minimal work units. But even the more successful approaches, such as Mulder's steady Euler equations solver (see [11, 12]), are still far less efficient than elliptic-system multigrid solvers, especially with high-order discretization schemes. This is due both to the time-stepping approach and to the slow convergence per time step, the main reasons for which are elaborated below and, from a different perspective, in [7].

There are usually a number of factors which contribute to increase the required work to large proportions. One of these is the insistence on reducing residuals to extremely small values rather than just the level of truncation errors. But as it is not the algebraic solution on the given grid that is sought, but rather the approximation to the differential solution, the lion's share of the invested effort does nothing to improve the solution. The amount of work needed to reduce residuals to such small values is usually quite large, whereas a 1FMG algorithm (described below) should normally suffice to obtain a solution that approximates the differential solution virtually as well.

The important first step in constructing a solver for the flow equations (indeed, for *any* complex problem) is the realization that the many different features associated with the problem need to be examined separately, numerically as well as analytically (see [4, Section 2.2]). Commonly chosen model problems, such as the driven cavity problem, include so many of these features (recirculation, boundary layers, singularities, poor approximation of some components), each of which requires its own special handling, that it is quite impossible to conclude from the results which of these is slowing down the solution process.

* Research supported in part by the Air Force Office of Scientific Research, United States Air Force, under Grants AFOSR-86-0127 and AFOSR-86-0126, and by the National Science Foundation under Grant NSF DMS-87-4169, and also by the Department of Energy under Contracts W-7405-ENG-36 and KC-07-01-01, while the second author was visiting the Center for Nonlinear Studies in the Los Alamos National Laboratory.

0021-9991/92 $5.00

Treatment of problems associated with singularities were introduced in [1] and applied to incompressible flow problems in [17]. Treatment of boundary layers is discussed in [4, Section 2.4], and problems associated specifically with recirculation are presented in [9]. The present research deals with the treatment of *entering flows*—flows with a well-defined general orientation that enter through some part of the boundary and leave through another. It is shown by analysis in Section 3 and by numerical experiments in Section 4 that, by employing relaxation in the downstream direction and thus using it as a *solver* rather than as a smoother for the non-elliptic part of the system, it is possible to obtain asymptotic convergence rates with second-order accurate discretization that are comparable to those obtained for the Poisson equation. Since this solution process essentially decouples the elliptic component of the system from the nonelliptic one and solves the latter directly, problems arising in cases of strong alignment of the flow with the grid (described in [2] and more explicitly in [12]) are eliminated. These results also suggest that more advanced methods, such as characteristic relaxation, can similarly be employed to obtain efficient solvers for steady-state and time-dependent problems with very little artificial diffusivity. These methods can be used in problems (or parts of problems), where the flows are of the entering type, while problems (or parts of problems), where the flow is separated or recirculates, are dealt with by other techniques, such as are presented in [7]), or possibly a combination of these techniques and the present approach, preliminary research of which appears in [8].

The method analyzed in Section 3 requires employment of an upstream difference scheme for the advective term. More precisely, the scheme must conserve the physical phenomenon of dependence (at the scale of the mesh-size) only on upstream data. If there is considerable *physical* viscosity on the scale of the grid, the present approach is no longer necessary, since the coarse grid will then provide a good correction of all smooth components. In the numerical experiments in Section 4 "narrow" upstream difference schemes are employed. While these are *not* an essential part of the approach, they are highly recommended, both due to their relatively small truncation errors (the flow being generally more nearly aligned with the grid) and due to the fact that the (linearized) equations remain locally decoupled at and near the outflow boundary without need of any extra processing. These points are elaborated in Section 4, Appendix A, and Appendix B.

In some applications, especially if the proposed methods are to be extended to compressible flows, it may be necessary to employ conservative schemes. Conservative upstream schemes are easily obtainable and appear in many publications. In particular, conservative *narrow* schemes have been developed and tested in [13–15], which can be employed in a similar fashion, although with somewhat greater complication in the implementation of the DGS relaxation.

2. THE MULTIGRID SOLVER

Consider the solution process of a single scalar equation, discretized by finite differences:

$$L^h u^h = f^h, \tag{1}$$

with appropriate boundary conditions. The classical *multigrid cycle for grid h* (the grid with mesh-size h), employing the *full approximation scheme* (FAS), is recursively defined as follows [2]:

1. Begin with some initial approximation to the solution on grid h. Smooth the error corresponding to this approximation by ν_1 relaxation sweeps, thereby decreasing the amplitude of error components of such high frequencies as cannot be approximated on the next coarser grid. The mesh-size of this coarse grid is normally chosen to be $2h$, and this is the convention below. The smoothed approximation is denoted by $\tilde{u}^h$.

2. Transfer the problem to the coarser grid. That is, solve the following problem on grid $2h$:

$$L^{2h}\hat{u}^{2h} = f^{2h} + \tau_h^{2h}, \tag{2}$$

where L^{2h} and f^{2h} are some coarse-grid approximations to L^h and f^h, respectively, and τ_h^{2h} is the fine-to-coarse defect correction defined as

$$\tau_h^{2h} = L^{2h}(\hat{I}_h^{2h}\tilde{u}^h) - I_h^{2h}(L^h\tilde{u}^h). \tag{3}$$

Here $\hat{I}_h^{2h}$ and I_h^{2h} are some fine-to-coarse transfer (restriction) operators, which need not be the same.

The approximate solution to the coarse-grid problem $\tilde{u}^{2h}$, with boundary conditions that approximate the fine-grid boundary conditions (including, generally, a τ correction similar to that at the interior), is obtained by γ multigrid cycles for grid $2h$, starting with the approximation $\hat{I}_h^{2h}\tilde{u}^h$. The solution on the coarsest grid is obtained either by some direct method or by repeated relaxation sweeps.

3. Interpolate and add the correction calculated on the coarse grid to the fine-grid approximation:

$$\tilde{u}_{\text{new}}^h = \tilde{u}^h + I_{2h}^h(\tilde{u}^{2h} - \hat{I}_h^{2h}\tilde{u}^h). \tag{4}$$

I_{2h}^h is a coarse-to-fine transfer (interpolation) operator, and $\hat{I}_h^{2h}$ must be the same as above.

4. Smooth the error again, employing ν_2 relaxation sweeps.

The multigrid cycle is thus characterized by three parameters: the number ν_1 of pre-relaxation sweeps, the number ν_2 of post-relaxation sweeps, and the "cycle index" γ. The cycle is denoted $V(\nu_1, \nu_2)$ if $\gamma = 1$ and $W(\nu_1, \nu_2)$ if $\gamma = 2$, reflecting the appearance of their respective flowcharts.

Multigrid cycles are usually incorporated into an outer process, the *FMG algorithm*, whose object is to enable the reduction of the *algebraic error* $u^h - \tilde{u}^h$ below the level of the *discretization error*, which is the difference between u^h and the solution to the differential equation. In the FMG algorithm the problem is first solved on the coarsest grid by repeated relaxations or direct solution and interpolated to the next finer grid. Now some number of multigrid cycles are performed, and the resulting solution is interpolated to a still finer grid. This process continues until a solution has been obtained on the finest grid desired. The number of multigrid cycles performed at each level before the solution is interpolated to a finer level characterizes the FMG algorithm. The aim is usually to obtain a final solution with a *1FMG algorithm*, that is, with a single multigrid cycle per level.

In many cases the 1FMG algorithm with V cycles suffices to yield a final solution with algebraic error that is much smaller than the discretization error. In some problems, however, the coarse grid does not approximate well certain components of the fine-grid solution. High-Reynolds flow problems, for example, where the discretization scheme will have some effective artificial diffusivity unless the flow is consistently aligned with the grid, fall into this category.

Consider the advection–diffusion equation

$$-\varepsilon \Delta u + \mathbf{a} \cdot \nabla u = 0 \tag{5}$$

over the full space, where $\varepsilon = 0^+$ (positive but infinitesimally small), and $\mathbf{a}$ is such that the characteristics are not consistently aligned with the grid. Here ∇ is the gradient operator and $\Delta = \nabla^2$ is the Laplacian. Suppose that the equation is discretized by a first-order upstream discretization. The viscosity term will then be roughly twice as large on the coarse grid as on the fine grid. A smooth characteristic error component, that is, one for which the reduced equation $\mathbf{a} \cdot \nabla u = 0$ is (nearly) satisfied, only receives about one half of the required correction, and the multigrid cycles used must therefore have an index γ of at least two in order to solve the coarse-grid equations sufficiently well, and even then its asymptotic convergence factor is 0.5 at best (see [3]). Nonetheless, a 1FMG algorithm still suffices to reduce the errors well below the discretization level. This is frequently the case in such problems, since the very same fine-grid components that the coarse grid approximates poorly are those for which the fine grid does not approximate the differential solution well. In higher-order discretizations, however, the discrepancy between the fine-grid error and its coarse-grid correction is even greater for such components. A greater γ is then required for the multigrid cycles, and also more than one multigrid cycle per level may then be necessary.

When the characteristics enter through the boundary, the problem of poor coarse-grid correction should be considered from a different point of view, as the influence of the inflow boundary must be brought into consideration. The most important factor in determining the quality of the coarse-grid correction is how well the smooth characteristic components with cross-stream frequency ω are advected from the inflow boundary into the domain. The main problem is again the increased numerical viscosity on the coarse grid, which causes a greater damping or smearing of these cross-stream components on the coarse grid than on the fine grid. As will be shown for the linearized flow equations in Section 3, a characteristic component with cross-stream frequency ω must suffer a numerical viscosity with an effective coefficient,

$$\varepsilon_{h,r}(\eta) = O(|\mathbf{a}|\, h^r \omega^{r-1}),$$

where r is the order of approximation. As a result, the component loses a substantial fraction of its amplitude at a distance

$$d_{h,r}(\omega) = O(\omega^{-r-1} h^{-r})$$

from the inflow boundary. This implies that the multigrid-cycle index γ should satisfy

$$\gamma \geqslant \frac{d_{h,r}(\omega)}{d_{2h,r}(\omega)} \approx 2^r,$$

for cross-stream component frequencies ω whose "survival distance" $d_{h,r}(\omega)$ is of the order of the domain size or smaller.

2.1. *Incompressible Flow Equations*

In the case of entering characteristics, the solution of (5) does not really require a multigrid process. By employing upstream discretization and performing the relaxation in a downstream ordering (piecewise, if necessary), the discretized equation can be solved in a single sweep. The incompressible Navier Stokes (INS) system, however, introduces several complications. In two dimensions the INS system can be written as

$$L\mathbf{u} = \begin{pmatrix} Q & 0 & \partial_x \\ 0 & Q & \partial_y \\ -\partial_x & -\partial_y & 0 \end{pmatrix} \begin{pmatrix} u \\ v \\ p \end{pmatrix} = \begin{pmatrix} f_1 \\ f_2 \\ f_3 \end{pmatrix}, \tag{6}$$

where u and v are the velocities in the x and y directions, respectively, p is the pressure, and the advection-diffusion operator Q is given by

$$Q = -\frac{1}{\mathrm{Re}}\Delta + u\partial_x + v\partial_y, \tag{6a}$$

Re being the Reynolds number.

One of these complications is the fact that we must deal with a system of coupled equations rather than a single equation. We must modify the relaxation process accordingly, so that relaxation of one equation will not affect the residuals of the others significantly (the alternative of relaxing the equations simultaneously, apart from being generally more expensive, is not well suited for the present application). A second complication is the nonlinearity. However, this is automatically treated by the use of FAS, and since it suffices to relax just the principal part of the system (i.e., to simply use some old values for u and v in (6a)), no linearization is necessary even in the relaxation (see [2]). The FMG algorithm plays an important role in obtaining a sufficiently good first approximation on the fine grid, which may be essential for convergence of the nonlinear problem. The operators on the coarser levels of this algorithm have large inherent viscosity coefficients, which gradually become smaller as finer grids are used. Thus, the FMG algorithm acts as a continuation process by gradually decreasing the measure of ellipticity and also gradually increasing the relative amplitude of the nonlinear terms. A third complication is the appearance of an elliptic component in the system:

$$\det L = Q\Delta. \tag{7}$$

The problem of smoothing is solved by employing distributive Gauss Seidel (DGS) relaxation [2, 6]. This entails an implicit change of variables that yields a triangular operator. It is formally done by multiplying L^h (the discrete form of L) from the right by a distribution operator M^h, given by

$$M^h = \begin{pmatrix} 1 & 0 & -\partial^h \\ 0 & 1 & -\partial^h \\ 0 & 0 & Q^h \end{pmatrix}, \tag{8}$$

yielding

$$L^h M^h = \begin{pmatrix} Q^h & 0 & 0 \\ 0 & Q^h & 0 \\ -\partial_x^h & -\partial_y^h & \Delta^h \end{pmatrix}, \tag{9}$$

where the h superscripts denote discrete approximations to the differential operators. Here the discretization of Δ is determined by that of ∂_x and ∂_y in L^h. On the staggered grid employed in the calculations presented in Section 4, L^h is equivalent to the usual five-point star discretization of the Laplacian. Thus an equivalent system is obtained with the triangular operator $L^h M^h$ and new variables $\hat{u}$, $\hat{v}$, and $\hat{p}$, whose relationship with the original variables is given by

$$\begin{pmatrix} u \\ v \\ p \end{pmatrix} = M^h \begin{pmatrix} \hat{u} \\ \hat{v} \\ \hat{p} \end{pmatrix}. \tag{10}$$

The resulting equations for the new variables are relaxed consecutively by Gauss Seidel relaxation, by introducing changes in the *original* variables as implied by the distribution operator M^h. This means that the momentum equations are relaxed first in the usual manner, but then the continuity equation is relaxed by changing several variables simultaneously as implied by (9) and (10). Examples are given in Section 4.

The asymptotic smoothing factor of the system (see, e.g., [2]) can be shown to be the largest of the smoothing factors of the operators on $\mathrm{diag}(L^h M^h)$. By employing upstream differencing and downstream marching, the smoothing factor of Q^h is almost reduced to 0, as the residuals are nearly eliminated for all components. Therefore, the overall smoothing rate is expected to be equal to that of the discrete Laplace operator.

3. TWO-LEVEL HALF-SPACE FMG MODE ANALYSIS

An analysis of the solution process must take into account the effects of the flow-entrance boundary. Therefore, the usual infinite-plane analysis that is commonly performed for elliptic systems is not appropriate. Instead, a half-space FMG mode analysis is performed. The analysis will incorporate the effects of special interest here, i.e., those of the potential malignant behavior, and for simplicity it will ignore others. Its full justification will be in the comparison with numerical experiments (Section 4). For a similar analysis for Eq. (5) see [3]. The general analytical approach is expounded in Sections 7.4 and 7.5 of [2].

3.1. *Linearized Equations*

In order to apply the mode analysis we must first linearize the flow equations. Let us therefore consider the following linearized steady incompressible flow equations with prescribed inflow velocities at the limit of very high Reynolds number over the half-space $x > 0$, $-\infty < y < \infty$,

$$\bar{L}\mathbf{u} = \begin{pmatrix} \bar{Q} & 0 & \partial_x \\ 0 & \bar{Q} & \partial_y \\ -\partial_x & -\partial_y & 0 \end{pmatrix} \begin{pmatrix} u \\ v \\ p \end{pmatrix} = 0, \tag{11}$$

with boundary conditions prescribed to be the Fourier component:

$$\begin{pmatrix} u \\ v \end{pmatrix}(0, y) = \begin{pmatrix} u_0 \\ v_0 \end{pmatrix} e^{i\omega y}. \tag{11a}$$

Here

$$\bar{Q} = -\varepsilon A + a\partial_x,$$

where a is a positive constant and $\varepsilon = 0^+$. Note that no generality is lost by choosing the characteristic direction to be x, since the orientation of the grid will be assumed to be general, and since the boundary ($x=0$) is arbitrary: we analyze and compare the development of the differential, the discrete, and the multigrid solutions starting at some imaginary line perpendicular to the flow. The analysis could be carried out also for a more general characteristic direction, but would not give an interestingly different comparison.

3.2. *Differential Solution*

We first calculate the differential solution to (11). Assuming it is of the form

$$\begin{pmatrix} u \\ v \\ p \end{pmatrix}(x, y) = \begin{pmatrix} u_0 \\ v_0 \\ p_0 \end{pmatrix} e^{-\alpha x + i\omega y},$$

we obtain

$$\begin{pmatrix} -\varepsilon(\alpha^2-\omega^2)-a\alpha & 0 & -\alpha \\ 0 & -\varepsilon(\alpha^2-\omega^2)-a\alpha & i\omega \\ \alpha & -i\omega & 0 \end{pmatrix} \begin{pmatrix} u_0 \\ v_0 \\ p_0 \end{pmatrix} = 0. \tag{12}$$

Therefore, the condition for a non-trivial solution (vanishing of the determinant) is

$$[-\varepsilon(\alpha^2-\omega^2)-a\alpha](\alpha^2-\omega^2) = 0. \tag{13}$$

Solving for α, while imposing the condition that the solution remain bounded as x tends to infinity (non-negative α) and neglecting high orders of ε, yields two values for α:

$$\alpha_1 \approx \varepsilon\omega^2/a \qquad \text{and} \qquad \alpha_2 = \omega.$$

The corresponding solution is therefore

$$\begin{pmatrix} u \\ v \\ p \end{pmatrix} = \left[A_1 \begin{pmatrix} 1 \\ -i\mu \\ 0 \end{pmatrix} e^{-\mu\omega x} + A_2 \begin{pmatrix} 1 \\ -i \\ -a \end{pmatrix} e^{-\omega x} \right] e^{i\omega y}, \tag{14}$$

with $\mu = \varepsilon\omega/a$ and, by (11a)

$$A_1 = \frac{u_0 - iv_0}{1-\mu}, \qquad A_2 = \frac{iv_0 - \mu u_0}{1-\mu}.$$

3.3. *Discrete Solution and Discretization Error*

We simplify the analysis of the discrete approximation to (11) by approximating the discrete advection operators by their first differential approximations (see [18, 3, or 2, Section 7.5]). For the other operators in (11), i.e., the pressure derivatives and the continuity-equation operator, we substitute the corresponding differential operators, under the assumption that the effect of the errors due to the discretization of these operators is small and benign compared to that of the advection-operator discretization (and is not the focus of our attention here). Moreover, we shall consider in our analysis only the limit of zero physical viscosity, which is the case for which the coarse-grid approximation of the fine-grid operator is generally the poorest (since the elliptic viscous terms are approximated very well), thereby reducing the calculations. Thus, an rth order upstream difference scheme $\bar{Q}^h$ approximating $\bar{Q}$ on grid h in the inviscid limit is represented by

$$\bar{Q}^h = -\varepsilon_h a T_{r+1}(\partial_x, \partial_y) + a\partial_x, \tag{15}$$

where the first term on the right-hand side represents the first truncated term in the discretization of $\bar{Q}$. T_{r+1} is a polynomial of degree $r+1$ of the form

$$T_{r+1}(\partial_x, \partial_y) = \sum_{j=0}^{r+1} a_j \partial_x^j \partial_y^{r+1-j} \tag{16}$$

and $|\varepsilon_h| = O(h^r)$. ε_h and the coefficients a_j are determined by the particular discretization and angle of nonalignment (remember that the flow is not aligned with the grid). Suppose, for example, that $a\partial_x$ is discretized on a Cartesian grid with coordinates $\tilde{x}$ and $\tilde{y}$, where the characteristic direction x is constant and forms an angle $0 \leqslant \varphi \leqslant \pi/2$ with $\tilde{x}$, so that

$$\partial_x = \cos\varphi\,\partial_{\tilde{x}} + \sin\varphi\,\partial_{\tilde{y}}.$$

Consider the standard first-order discretization as defined in (35). The first terms in the truncation error of this discretization of ∂_x are

$$-\frac{h}{2}(\cos\varphi\,\partial_{\tilde{x}\tilde{x}} + \sin\varphi\,\partial_{\tilde{y}\tilde{y}}).$$

Transferring back to the characteristic coordinates we find the corresponding $\varepsilon_h T_2$ to be given by

$$\begin{aligned} \varepsilon_h T_2(\partial_x, \partial_y) = \frac{h}{2}[&\sin\varphi\cos\varphi(\sin\varphi + \cos\varphi)\,\partial_{yy} \\ &+ 2\sin\varphi\cos\varphi(\sin\varphi - \cos\varphi)\,\partial_{xy} \\ &+ (\cos^3\varphi + \sin^3\varphi)\,\partial_{xx}]. \end{aligned}$$

A "narrow" scheme, the diameter of whose stencil on a plane perpendicular to the characteristic direction is small compared to that of the standard schemes, will generally have a smaller corresponding $|\varepsilon_h|$. For convenience we choose ε_h so that $a_0 = 1$, e.g., $\varepsilon_h = (h/2)\sin\varphi\cos\varphi(\sin\varphi + \cos\varphi)$ in the example above. This is only possible if the highest cross-stream derivative in the truncation error does not vanish, as happens when there is consistent alignment of the flow with the grid (e.g., when $\cos\varphi$ or $\sin\varphi$ vanish in the example above), and also in certain nonaligned cases (see Appendix A). In these cases, however, the coarse grid approximates the fine-grid solution well for all components, so the troubles investigated here do not appear.

The solution on grid h satisfies (12) with $(\alpha^2 - \omega^2)$ replaced by $T_{r+1}(-\alpha, i\omega)$, and ε replaced by $a\varepsilon_h$. The condition for non-trivial solution is now

$$[-\varepsilon_h a T_{r+1}(-\alpha, i\omega) - a\alpha](\alpha^2 - \omega^2) = 0. \tag{17}$$

Once more we consider only solutions which remain bounded as $x \to \infty$. The second factor in (17) therefore yields $\alpha_2 = \omega$. The first factor may have up to $r+1$ roots, but simple dimensional analysis shows that the absolute values of all but one of these are $O(|\varepsilon_h|^{-1/r}) = O(1/h)$. When the real part of α is large and negative such values imply instability (or perhaps a boundary layer near the outflow boundary in a finite domain). When α is purely imaginary, they imply spurious oscillations. Finally, if the real part of α is large and positive, such components decay very close to the inflow boundary. Hence, the relevant roots are

$$\alpha_1 \approx -\varepsilon_h (i\omega)^{r+1}, \qquad \alpha_2 = \omega,$$

and the solution is

$$\begin{pmatrix} u^h \\ v^h \\ p^h \end{pmatrix} = \left[A_1^h \begin{pmatrix} 1 \\ -i\mu_h \\ 0 \end{pmatrix} e^{-\mu_h \omega x} + A_2^h \begin{pmatrix} 1 \\ -i \\ a(\mu_h s_{r+1} - 1) \end{pmatrix} e^{-\omega x} \right] e^{i\omega y}, \tag{18}$$

with $\mu_h = -\varepsilon_h (i\omega)^{r+1}/\omega$ and

$$s_{r+1} = \frac{T_{r+1}(-\omega, i\omega)}{(i\omega)^{r+1}} = \sum_{j=0}^{r+1} i^j a_j,$$

$$A_1^h = \frac{u_0 - iv_0}{1 - \mu_h}, \qquad A_2^h = \frac{iv_0 - \mu_h u_0}{1 - \mu_h}.$$

Note that a stable scheme requires ε_h to be such that the real part of μ_h is nonnegative.

The second term in solution (18) loses most of its amplitude at distance $O(\omega^{-1})$ from the boundary, and for most frequencies it quickly becomes much smaller than the first term. The first term's "survival distance" is $O(\mu_h^{-1}\omega^{-1}) = O(\omega^{-r-1}h^{-r})$, as noted in Section 2.

The *discretization error* is defined as the difference between the differential solution (14) and the discrete solution (18).

3.4. *Multigrid Solver and Algebraic Error*

Next we will calculate the approximation to the differential solution (14) obtained by the two-level 1FMG algorithm, defined by the following steps:

1. Obtain an approximation to the differential solution on the coarse grid (mesh-size $2h$) by solving the equations resulting from the coarse-grid discretization.
2. Interpolate the solution to the fine grid (mesh-size h).
3. Perform v_1 DGS sweeps. In each sweep the momentum equations are relaxed first, or rather integrated in downstream ordering with a fixed pressure field in the first sweep. Then the continuity equation is relaxed, while the momentum equation residuals remain unaffected. This property is not satisfied near the inflow boundary, and it may be advisable to follow up the continuity-equation relaxation with another sweep of the momentum equations (see Section 4.2).
4. Calculate the residuals of the continuity equation and transfer them to the corresponding right-hand sides on the coarse grid with some suitable restriction operator. The momentum-equation residuals need not be transferred, as they are negligibly small compared to the continuity-equation residuals after the final momentum-equation sweep.
5. Solve for the corrections on the coarse grid.
6. Interpolate the corrections to the fine grid and add them to the current fine-grid approximation.
7. Perform v_2 DGS sweeps.

We simplify the analysis of this algorithm by neglecting errors introduced by the inter-grid transfers. For elliptic problems their effect can be shown to be small if they are of the proper order (see [5]). In the present system some of the assumptions in [5] do not hold. Full inclusion of the inter-grid transfers in the present FMG analysis can be accomplished for a finite number of levels by taking into account the coupling of modes (much the same as in the usual full-space two-level analysis). But such an undertaking is only reasonable if the effect of relaxation is also included (since high-frequency errors are then also considered), leading to very complicated calculations which would obscure rather than clarify the main issue: the problem of poor coarse-grid

correction to smooth characteristic components and its solution.

When the coarse grid solution is interpolated to the fine grid, the initial *algebraic error* in the pressure on the fine grid, defined as the difference between the current approximation (obtained from the coarse grid) and the discrete solution (18) is

$$E_p^h = p^{2h} - p^h = a\mu_h K_h e^{-\omega x + i\omega y},$$

where p^{2h} is the pressure field as given by (18) with μ_h replaced by $\mu_{2h} = -\varepsilon_{2h}(i\omega)^{r+1}/\omega$ and

$$K_h = \frac{\begin{pmatrix}(\xi-1)[u_0 - iv_0 \\ \quad + s_{r+1}(iv_0 - \mu_h u_0(\xi+1) + (\mu_h)^2 u_0 \xi)]\end{pmatrix}}{(1-\xi\mu_h)(1-\mu_h)},$$

with $\xi = \varepsilon_{2h}/\varepsilon_h \approx 2^r$.

Now, after a sweep over the momentum equations is performed on the fine grid, the algebraic errors in the velocities satisfy

$$\bar{Q}^h E_u^h = -\partial_x E_p^h, \qquad \bar{Q}^h E_v^h = -\partial_y E_p^h, \tag{19}$$

with boundary conditions $E_u^h = E_v^h = 0$ at $x = 0$. Here

$$E_u^h = \tilde{u}^h - u^h, \qquad E_v^h = \tilde{v}^h - v^h,$$

with $\tilde{u}^h$, $\tilde{v}^h$ denoting current approximations on the fine grid and u^h, v^h as the exact solutions of the fine-grid equations. Integration of (19) yields

$$E_u^h = \frac{\mu_h K_h}{1-\mu_h s_{r+1}}(e^{-\mu_h\omega x} - e^{-\omega x})\, e^{i\omega y},$$

$$E_v^h = -\frac{i\mu_h K_h}{1-\mu_h s_{r+1}}(e^{-\mu_h\omega x} - e^{-\omega x})\, e^{i\omega y},$$

where we have again assumed that solutions with $O(1/h)$ frequencies do not appear. A single sweep of the momentum equations suffices to obtain these values for the algebraic errors in the velocities, since these equations are integrated in a downstream direction.

Now the continuity equation is relaxed ν_1 times with DGS relaxation. This does not affect the residuals of the momentum equations (except near the inflow boundary), and we also neglect in the present analysis the effect of this relaxation on the velocity-error components. Since we are only dealing with smooth error components, the effect of the relaxation on these components is very small. The residuals of the continuity equation after the fine-grid sweep are therefore

$$R_c^h = \partial_x E_u^h + \partial_y E_v^h = \frac{\omega\mu_h K_h}{1-\mu_h s_{r+1}}(1-\mu_h)\, e^{-\mu_h\omega x + i\omega y}, \tag{20}$$

while the residuals of the momentum equations are 0. The residuals of the continuity equation are transferred to the coarse grid, and the resulting coarse grid equations for the correction are

$$\bar{L}^{2h}\begin{pmatrix} C_u^{2h} \\ C_v^{2h} \\ C_p^{2h}\end{pmatrix} = \begin{pmatrix} 0 \\ 0 \\ R_c^h\end{pmatrix}, \tag{21}$$

with $C_u^{2h} = C_v^{2h} = 0$ at the inflow boundary. Here $\bar{L}^{2h}$ is the coarse-grid approximation to $\bar{L}$ in which we again approximate the advection operator with the first differential approximation as in (15), with ε_h replaced by $\varepsilon_{2h} = \xi\varepsilon_h$, while the other discrete operators are again approximated by their corresponding differential operators.

This system is satisfied by

$$\begin{pmatrix} C_u^{2h} \\ C_v^{2h} \\ C_p^{2h}\end{pmatrix} = \frac{\mu_h K_h}{1-\mu_h s_{r+1}}\left[B_1 \begin{pmatrix} 1 \\ -i\xi\mu_h \\ 0\end{pmatrix} e^{-\xi\mu_h\omega x} + B_2 \begin{pmatrix} 1 \\ -i \\ a(\xi\mu_h s_{r+1} - 1)\end{pmatrix} e^{-\omega x} + B_3 \begin{pmatrix} \mu_h \\ -i \\ a\mu_h(\xi-1)\end{pmatrix} e^{-\mu_h\omega x}\right] e^{i\omega y}, \tag{22}$$

with B_1, B_2, and B_3 determined by the boundary conditions and the right-hand side to be

$$B_1 = \frac{\mu_h - 1}{(1-\xi\mu_h)(1+\mu_h)},$$

$$B_2 = \frac{1-\xi(\mu_h)^2}{(1-\xi\mu_h)(1+\mu_h)}, \qquad B_3 = \frac{-1}{1+\mu_h}.$$

Accordingly, the algebraic error in the pressure after the correction is added is

$$E_p^h \leftarrow E_p^h + C_p^{2h} = \frac{aK_h(\mu_h)^2}{1-\mu_h s_{r+1}}\left(\frac{(\xi-1)(s_{r+1}-1)}{(1-\xi\mu_h)(1+\mu_h)} e^{-\omega x} - \frac{\xi-1}{1+\mu_h} e^{-\mu_h\omega x} + O(\mu_h)\right) e^{i\omega y}.$$

The error in the pressure is seen to be reduced to $O((\mu_h)^2)$. After another sweep of the momentum equations, this holds for the velocities as well. Also, the ratio between this algebraic error and the discretization error of the velocities is $O(\mu_h)$ for all values of ω and x; e.g., the discretization error corresponding to u^h, calculated from

the difference between (14) and (18), is proportional to $1-e^{-\mu_h \omega x} = O(\mu_h \omega x)$ (plus higher-order terms in μ_h), whereas integration of the x derivative of the new pressure error yields at worst $O((\mu_h)^2 \omega x)$. Since only components for which $\mu_h \ll 1$ are approximated well by the scheme, having survival distances of more than just a few mesh-sizes, this implies that the algebraic error is reduced well below the discretization error for all relevant components.

4. NUMERICAL EXPERIMENTS

The prediction of the half-space analysis was tested by numerical solution of the INS system (6) with 0 right-hand side on the unit square $[0, 1] \times [0, 1]$. At the inflow boundary, the velocities u and v were prescribed to be of the form

$$u(0, y) = F_i(y) \qquad v(0, y) = v_0 F_i(y). \tag{23}$$

Several functions $F_i(y)$ were tested, leading to solutions with varying degrees of smoothness:

$$F_1(y) = 1 + 0.5 \sin(2\pi y)$$

$$F_2(y) = 1 + \begin{cases} 0.5, & 0.25 < y \leqslant 0.75 \\ 0, & \text{otherwise} \end{cases}$$

$$F_3(y) = \begin{cases} 2y - 0.5, & 0.25 < y \leqslant 0.5 \\ 1.5 - 2y, & 0.5 < y \leqslant 0.75 \\ 0, & \text{otherwise} \end{cases}$$

$$F_4(y) = 1 + \begin{cases} 16y^2 - 8y + 1, & 0.25 < y \leqslant 0.375 \\ -16y^2 + 16y - 3.5, & 0.375 < y \leqslant 0.625 \\ 16y^2 - 24y + 9, & 0.625 < y \leqslant 0.75 \\ 0, & \text{otherwise.} \end{cases}$$

Note that F_1 is analytic, F_2 is discontinuous, F_3 is in C_0, and F_4 in C_1. Also, several different values of v_0 were tried in order to test the effect of the angle of non-alignment.

The outflow boundary condition in all the calculations was

$$p(1, y) = 0,$$

and periodic boundary conditions were imposed at $(x, 0)$ and $(x, 1)$:

$$\begin{pmatrix} u \\ v \\ p \end{pmatrix}(x, y+1) = \begin{pmatrix} u \\ v \\ p \end{pmatrix}(x, y).$$

This choice of periodic boundary conditions is very important, as it precludes boundary layers which might obscure the phenomena examined here. Also, it facilitates control of the angle of non-alignment.

The exact solution to the reduced system, i.e., in the inviscid limit, is

$$\begin{aligned} &u(x, y) = F_i(y - v_0 x), \\ &v(x, y) = v_0 F_i(y - v_0 x), \qquad p(x, y) = 0. \end{aligned} \tag{24}$$

4.1. *Discretization*

The equations were discretized on a square staggered grid as in [2] (see Fig. 1). The p variables are located at cell centers, and also in the outflow boundary, where they are located at the centers of the vertical cell sides. The u variables are located at the centers of the vertical cell-sides and the v variables at the centers of the horizontal cell-sides, and also in the inflow boundary, where they are located at the nodes. Thus, $p_{i,j}$ is located at point $(h(i-\frac{1}{2}), h(j+\frac{1}{2}))$ in the interior and also at $(1, h(j+\frac{1}{2}))$ in the outflow boundary; $u_{i,j}$ is located at $(hi, h(j+\frac{1}{2}))$ everywhere, and $v_{i,j}$ is located at $(h(i-\frac{1}{2}), hj)$ in the interior and at $(0, hj)$ in the inflow boundary.

The continuity equation is centered at the cell-centers and discretized by *short* (i.e., based on distance h, not $2h$) second-order differences. The x and y momentum equations are centered at the u and v locations, respectively, and discretized by narrow upstream differencing (NUD) for the advection terms, with short central differencing for the p derivatives except p_x at the outflow boundary, which is discretized by upstream differences due to the changed location of p. The general NUD is defined in Appendix A. In the present problem, where u, v, and $u-v$ are positive

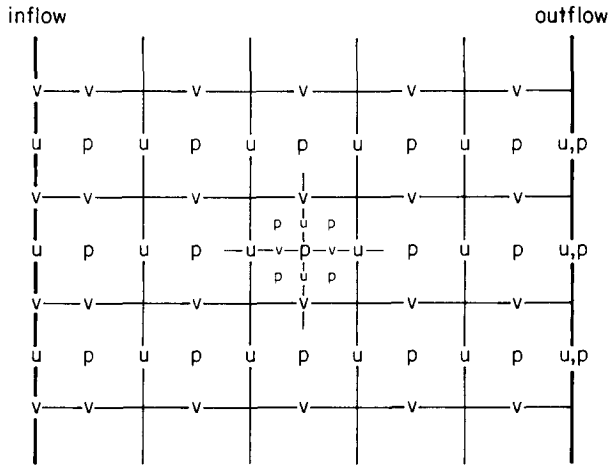

FIG. 1. A part of the grid is shown, including the inflow and outflow boundaries. The variables in small print are examples of those defined on the next-finer grid.

throughout the domain, first-order NUD for the advection of u in multiplied form is defined by

$$h(uu_x + vu_y)^h_{i,j} = (u_{i,j} - \tilde{v}_{i,j})(u_{i,j} - u_{i-1,j}) + \tilde{v}_{i,j}(u_{i,j} - u_{i-1,j-1}), \quad (25)$$

where $\tilde{v}_{i,j}$ is an interpolated value for $v_{i,j}$, given by

$$\tilde{v}_{i,j} = 0.25(v_{i,j} + v_{i+1,j} + v_{i,j+1} + v_{i+1,j+1}) \quad (26)$$

except at the outflow boundary, where $\tilde{v}_{i,j}$ is extrapolated linearly rather than interpolated. Here and below, all operations with respect to j are understood to be modul n, where $n = 1/h$ is the height of the domain in mesh-intervals, thereby imposing periodicity.

The first-order NUD scheme for the advection of v is similarly defined except near the inflow boundary where, due to the location of v at the boundary, it is modified to

$$0.5h(uv_x + vv_y)^h_{1,j} = (\tilde{u}_{1,j} - v_{1,j})(v_{1,j} - v_{0,j}) + v_{1,j}(v_{1,j} - v_{0,j-1/2}), \quad (27)$$

with $\tilde{u}$ given by

$$\tilde{u}_{i,j} = 0.25(u_{i,j} + u_{i-1,j} + u_{i,j-1} + u_{i-1,j-1}). \quad (28)$$

Here $v_{0,j-1/2}$ is the value of v at point $(0, h(j-1/2))$, which can be approximated by linear interpolation is it is not explicitly given.

Second-order NUD for the advection of u under the conditions of our experiments is defined by

$$h(uu_x + vu_y)^h_{i,j} = (u_{i,j} - \tilde{v}_{i,j})(1.5u_{i,j} - 2u_{i-1,j} + 0.5u_{i-2,j}) + \tilde{v}_{i,j}(1.5u_{i,j} - 2u_{i-1,j-1} + 0.5u_{i-2,j-2}), \quad (29)$$

with $\tilde{v}_{i,j}$ and p_x as in the first-order scheme. At $i = 1$ this scheme must be modified, since the variables are not defined at points with negative values of i. There are a number of ways by which second-order accuracy can be maintained at these points, and the choice is influenced mainly by the behavior of the DGS relaxation. Near the inflow boundary it is no longer true that DGS relaxation of the continuity equation leaves the residuals of the principal part of the momentum equations unaffected, and the choice of discretization there should be such that this causes minimal damage. We have found the scheme described in Appendix B, which is compact in the x direction, to be good in this respect, and the numerical results presented were calculated using this scheme. However, other means, such as defect corrections at these points, can be employed instead.

Second-order NUD is again similarly defined for advection of v, but must now be modified at $i = 1$ and $i = 2$. At $i = 2$ the resulting scheme is

$$3h(uv_x + vv_y)^h_{2,j} = (\tilde{u}_{2,j} - v_{2,j})(5v_{2,j} - 9v_{1,j} + 4v_{0,j}) + v_{2,j}(5v_{2,j} - 9v_{1,j-1} + 4v_{0,j-3/2}). \quad (30)$$

Here $v_{0,j-3/2}$ is the value of v at point $(0, h(j-\frac{3}{2}))$, which must be interpolated by quadratic interpolation if it is not explicitly given. At $i = 1$ we again employ a scheme that is compact in the x direction which is also described in Appendix B.

The narrow schemes have at least two advantages over the standard first-order and second-order upstream schemes (SUD), which are also defined in Appendix A. One advantage is a considerably smaller local truncation error. On the average, these schemes yield as good an approximation as can be obtained on a twice finer grid by standard upstream differencing and are only marginally more expensive (see Appendix A). This holds both for the first-order and second-order schemes. The second advantage of the NUD schemes is in the treatment at the outflow boundary. When such a scheme is employed for the x momentum equation at a certain outflow boundary point, no u variable at any other boundary point is included in the discretization. As a result, the DGS relaxation can be modified near the outflow boundary so as to maintain the property that the residuals of the principal part of the momentum equations are not affected by relaxation of the continuity equation (see Fig. 3 in Appendix B).

4.2. *Relaxation and Inter-grid Operators*

The DGS relaxation is performed as follows: first the x and y momentum equations are scanned and the corresponding values of u and v are changed so as to satisfy these equations (it is sufficient to use old values for the coefficient in the advection operators). This is done in downstream ordering and serves to nearly eliminate the momentum equation residuals. Then the continuity equations are scanned in same order and the equation at each point in turn is satisfied by introducing the changes described in Fig. 2, as implied by the distribution operator M^h in (8). Near the boundaries these changes must be altered, since the discretizations are slightly different. The rule we followed in our numerical experiments was to make the changes near the boundaries such that the principal part of the y momentum equations remain unchanged. Also, when the equation is relaxed at points near the outflow boundary, changes are introduced in the boundary values of u that keep the principal part of the x momentum equations there unchanged as well (see Fig. 3 in Appendix B). Hence, only near the inflow boundaries does the sweep of the continuity

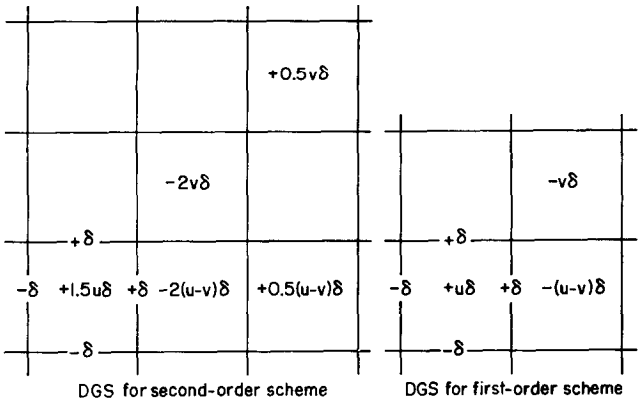

FIG. 2. Distributive Gauss Seidel relaxation at interior points for the case that u, v, and $u - v$ are nonnegative. Shown are the changes introduced in the variables at the corresponding locations. $\delta = hR/4$, where R is the residual of the continuity equation defined at the center of the lower left-hand cell.

equation perturb the x momentum equations significantly. But if the sweep of the continuity equation is followed by another downstream sweep of the momentum equations, the feedback in terms of continuity-equation residuals is very slight. Indeed, this feedback can be shown to be zero in the aligned case $v = 0$ and also in the case where the perturbation in the momentum-equation residuals due to the DGS sweep near the boundaries is very smooth in the y direction. Accordingly, the numerical results are improved when the momentum equations are swept again before the residuals are transferred to the coarse grid, and there is no increase in the overall cost, since it is not necessary now to transfer residuals of the momentum equations to the coarse grid, because they are now negligibly small compared with those of the continuity equation.

In the experiments residuals were transferred to the coarse grid by full weighting. Interpolation of the *solution* was bi-cubic. For the *corrections*, bi-linear interpolation yielded results that were as good as those with bi-cubic interpolation.

4.3. *Results*

Asymptotic convergence rates were tested on a linearized system, since the solution can then be chosen to be zero, avoiding the problem of round-off errors. Also, with the linearized system it was possible to test the performance with curved characteristics without introducing boundary layers. The behavior of the full equations, however, was very similar until (double-precision) round-off errors were encountered. The "effective smoothing rate," defined as the convergence rate per fine-grid relaxation sweep, was calculated for $W(1, 1)$, $W(2, 1)$, and $V(1, 1)$ cycles with the first-order and second-order schemes. The corresponding values were found to be 0.53, 0.60, and 0.78 for the three cycle-types, respectively, and first-order NUD discretization, and 0.55, 0.61, and 0.80 with second-order NUD discretization. These results were achieved with bi-linear interpolation of the corrections and lexicographic ordering of relaxation of the continuity equation. The results with bi-cubic interpolation and also with red–black ordering of the continuity equation relaxation were very similar. The effect of the angle of non-alignment on these values was small. The finest mesh-size in these experiment was $\frac{1}{128}$, and six levels were employed. The experiments with the linear system were performed with a coefficient of one for the x derivative in the advection terms and $0.5 \cos^2(l\pi x)$ for the y derivative, with various values for l, in order to test the effect of curved characteristics. The asymptotic convergence rates quoted above hold for small and moderate values of l. Only when l approaches $1/h$ (corresponding to a substantial difference in the velocity at adjacent grid-locations in the nonlinear case), does the performance begin to deteriorate.

These results indicate that it is better to use a W cycle than a V cycle. Still larger values of the index γ did not improve the performance, however. Even then, the results are not quite as good as the 0.50 factor that is predicted by smoothing rate analysis of the Poisson equation discretized by the usual five-point star, to which the DGS scheme with the staggering we have employed is equivalent. This seems to be due to the treatment near the inflow boundary. Extra relaxation near the boundary, however, yields very little improvement in the asymptotic convergence rates. It should be noted that the performance of the $W(1, 1)$ cycles only dropped below that of the Poisson-equation solver after the error had been reduced by about 20 orders of magnitude, and so the reduced performance is of no practical importance.

We remark here that fairly similar performance has been reported for flow in a duct in [10], albeit only with first-order accurate discretization (in three dimensions). The authors, however, had overlooked the main issue, which is the effect of non-alignment, and chose flow that was nearly aligned with the grid in their experiments. Also, the crucial question of the order in which the momentum equations are relaxed is not addressed. Finally, the grids on which the results were achieved were extremely coarse, and the multigrid cycles employed only two or three levels. Thus, the actual viscosity in the scheme used is very much greater than that implied by the Reynolds numbers.

The performance of a 1FMG algorithm for the full equations was tested with the four different inflow-boundary conditions F_1–F_4 listed above, each with three values of v_0—0.1, 0.25, and 0.5. The results are listed in Tables I and II for the first-order and second-order approximations, respectively. The first column lists the mesh-size to which the results correspond, the second column shows the inflow condition, the third gives the degree of non-alignment (in effect, the tangent of the angle between the flow and the x-gridlines). In the fourth column is the L_2 norm of the dis-

TABLE I

1FMG with First-Order Discretization

h	F_i	v_0	$\|e_d\|_2$	$\|e_a\|_2/\|e_d\|_2$		
			Type of cycle—	$W(2,1)$	$W(1,1)$	$V(2,1)$
1/32	F_1	0.10	8.49×10^{-3}	0.113	0.131	0.536
1/64	F_1	0.10	4.21×10^{-3}	0.032	0.042	0.839
1/128	F_1	0.10	2.10×10^{-3}	0.013	0.018	1.162
1/32	F_1	0.25	1.77×10^{-2}	0.113	0.140	0.490
1/64	F_1	0.25	8.85×10^{-3}	0.037	0.051	0.743
1/128	F_1	0.25	4.43×10^{-3}	0.016	0.021	1.034
1/32	F_1	0.50	2.46×10^{-2}	0.104	0.160	0.375
1/64	F_1	0.50	1.24×10^{-2}	0.042	0.067	0.569
1/128	F_1	0.50	6.20×10^{-3}	0.018	0.027	0.856
1/32	F_2	0.10	6.59×10^{-2}	0.018	0.022	0.023
1/64	F_2	0.10	5.49×10^{-2}	0.021	0.024	0.035
1/128	F_2	0.10	4.61×10^{-2}	0.022	0.023	0.044
1/32	F_2	0.25	7.88×10^{-2}	0.022	0.034	0.044
1/64	F_2	0.25	6.58×10^{-2}	0.023	0.030	0.051
1/128	F_2	0.25	5.55×10^{-2}	0.020	0.021	0.047
1/32	F_2	0.50	8.55×10^{-2}	0.023	0.052	0.036
1/64	F_2	0.50	7.12×10^{-2}	0.020	0.043	0.035
1/128	F_2	0.50	6.01×10^{-2}	0.018	0.027	0.031
1/32	F_3	0.10	1.22×10^{-2}	0.026	0.026	0.073
1/64	F_3	0.10	7.16×10^{-3}	0.013	0.013	0.095
1/128	F_3	0.10	4.25×10^{-3}	0.007	0.007	0.108
1/32	F_3	0.25	2.07×10^{-2}	0.031	0.032	0.074
1/64	F_3	0.25	1.22×10^{-2}	0.016	0.016	0.091
1/128	F_3	0.25	7.24×10^{-3}	0.008	0.008	0.100
1/32	F_3	0.50	2.62×10^{-2}	0.031	0.037	0.062
1/64	F_3	0.50	1.53×10^{-2}	0.017	0.019	0.073
1/128	F_3	0.50	9.06×10^{-3}	0.009	0.010	0.088
1/32	F_4	0.10	1.43×10^{-2}	0.036	0.038	0.086
1/64	F_4	0.10	7.43×10^{-3}	0.021	0.022	0.126
1/128	F_4	0.10	3.81×10^{-3}	0.011	0.012	0.164
1/32	F_4	0.25	2.59×10^{-2}	0.038	0.042	0.079
1/64	F_4	0.25	1.43×10^{-2}	0.022	0.021	0.106
1/128	F_4	0.25	7.58×10^{-3}	0.013	0.013	0.129
1/32	F_4	0.50	3.28×10^{-2}	0.037	0.048	0.064
1/64	F_4	0.50	1.85×10^{-2}	0.024	0.023	0.081
1/128	F_4	0.50	1.00×10^{-2}	0.014	0.014	1.105

TABLE II

1FMG with Second-Order Discretization

h	F_i	v_0	$\|e_d\|_2$	$\|e_a\|_2/\|e_d\|_2$		
			Type of cycle—	$W(2,1)$	$W(1,1)$	$V(2,1)$
1/32	F_1	0.10	9.52×10^{-4}	0.056	0.151	0.223
1/64	F_1	0.10	2.18×10^{-4}	0.033	0.097	0.216
1/128	F_1	0.10	4.77×10^{-5}	0.024	0.111	0.339
1/32	F_1	0.25	1.12×10^{-3}	0.108	0.231	0.434
1/64	F_1	0.25	2.61×10^{-4}	0.063	0.172	0.569
1/128	F_1	0.25	6.10×10^{-5}	0.038	0.232	0.660
1/32	F_1	0.50	9.85×10^{-4}	0.353	0.430	0.526
1/64	F_1	0.50	1.99×10^{-4}	0.147	0.293	2.095
1/128	F_1	0.50	2.61×10^{-5}	0.154	0.524	3.943
1/32	F_2	0.10	5.52×10^{-2}	0.022	0.036	0.022
1/64	F_2	0.10	4.60×10^{-2}	0.036	0.054	0.042
1/128	F_2	0.10	3.77×10^{-2}	0.067	0.087	0.088
1/32	F_2	0.25	5.80×10^{-2}	0.037	0.053	0.046
1/64	F_2	0.25	4.77×10^{-2}	0.086	0.103	0.110
1/128	F_2	0.25	3.96×10^{-2}	0.161	0.203	0.204
1/32	F_2	0.50	6.19×10^{-2}	0.109	0.121	0.140
1/64	F_2	0.50	4.60×10^{-2}	0.159	0.211	0.192
1/128	F_2	0.50	3.55×10^{-2}	0.571	0.916	0.698
1/32	F_3	0.10	6.27×10^{-3}	0.013	0.020	0.022
1/64	F_3	0.10	3.31×10^{-3}	0.012	0.019	0.019
1/128	F_3	0.10	1.75×10^{-3}	0.013	0.018	0.018
1/32	F_3	0.25	7.23×10^{-3}	0.022	0.032	0.049
1/64	F_3	0.25	3.82×10^{-3}	0.030	0.040	0.050
1/128	F_3	0.25	2.04×10^{-3}	0.033	0.040	0.049
1/32	F_3	0.50	6.13×10^{-3}	0.059	0.078	0.103
1/64	F_3	0.50	2.66×10^{-3}	0.104	0.143	0.138
1/128	F_3	0.50	1.17×10^{-3}	0.132	0.178	0.170
1/32	F_4	0.10	4.45×10^{-3}	0.026	0.027	0.049
1/64	F_4	0.10	1.42×10^{-3}	0.028	0.036	0.047
1/128	F_4	0.10	4.64×10^{-4}	0.028	0.044	0.058
1/32	F_4	0.25	5.36×10^{-3}	0.067	0.082	0.124
1/64	F_4	0.25	1.74×10^{-3}	0.054	0.048	0.076
1/128	F_4	0.25	5.77×10^{-4}	0.040	0.042	0.117
1/32	F_4	0.50	3.24×10^{-3}	0.269	0.343	0.411
1/64	F_4	0.50	7.89×10^{-4}	0.265	0.326	0.330
1/128	F_4	0.50	1.68×10^{-4}	0.288	0.391	0.701

cretization error of u, which is defined as the difference between the exact solution (24) to the inviscid differential problem and the algebraic solution on the corresponding grid, calculated by performing many cycles in order to reduce the residuals to round-off error level. Note that in the smooth problems the discretization error is indeed roughly proportional to h and h^2 for first-order and second-order discretizations, respectively, except for the maximally non-aligned case and second-order discretization, where analysis shows that the first cross-stream truncation term of second-order NUD vanishes, yielding a higher-order scheme (see Appendix A). Columns five through seven show the ratio between the L_2 norm of the algebraic error yielded by a 1FMG algorithm (that is, the difference between the solution obtained with a 1FMG algorithm and the round-off error solution) and the L_2 norm of the discretization error of u that is listed in the fourth column.

It is evident that for smooth and non-smooth solutions alike, *a 1FMG algorithm suffices to reduce the algebraic error well below the level of the discretization error.* Also, for first-order discretization, the prediction of the analysis that their ratio be proportional to the mesh-size is realized. For the contact-discontinuity condition F_2 this does not hold, but then it is not implied by the analysis either, since components with $\mu_h = O(1)$ have a substantial amplitude. The predicted behavior is not obtained with the $V(2,1)$ cycle,

although the corresponding results are still mostly satisfactory as far as reduction of the algebraic errors is concerned.

In the results with second-order discretization depicted in Table II, the 1FMG cycle again performs very satisfactorily. The ratio between the algebraic and discretization errors does not now behave quite as predicted. This is due to the fact that the discretization error of the continuity equation is now significant, a factor which was neglected in the analysis of Section 3. When $v_0 = 0.5$ the performance seems to weaken somewhat. The reason for this is that in this maximally non-aligned case, the second-order term in the truncation error of the NUD scheme vanishes, yielding a higher-order scheme as noted above and shown in Appendix A. Now the local truncation error is determined by the discretization of the continuity equation (note in column four that the discretization error with $v_0 = 0.5$ is smaller than the nearly aligned case $v_0 = 0.1$). The seemingly somewhat worse performance (in reducing algebraic error far below truncation errors) is of no importance, as it is due to an "accidental" drop in the truncation error.

There is a slight weakening in performance of the 1FMG algorithm with second-order discretization in the case of contact discontinuity. The approximation is then far from second-order, as is well known and can also be gauged by examining the fourth column. This weakening in performance is typical in multigrid processes when bad discretization is used and should always serve as a warning sign. There are a number of methods that have been developed by researchers for dealing with the problem of poor discretization near discontinuities, many of which may be combined with the approach we have presented. Our present research in this direction is outlined below.

5. CONCLUSIONS AND FUTURE RESEARCH

The analysis and experiments have confirmed that it is indeed possible to separate between the elliptic and non-elliptic components of the flow equations in the solution process, enabling the use of downstream relaxation as a fast solver for a non-elliptic factor in the equations as part of an overall multigrid algorithm.

A natural next step is to carry out the relaxation of the momentum equations along characteristics, thereby reducing the artificial viscosity drastically. The advected values are then interpolated to a fixed cartesian grid which serves several functions: it is used for multigrid solution of the continuity equation; physical viscosity (which is treated as a right-hand side) can be calculated from the grid-values; it serves as a "backbone" from which calculation can be restarted, should the characteristics that are being followed by the relaxation become too tangled or dense. The overall artificial viscosity introduced by such a scheme is very small, even if one must make a few such restarts. This method seems to be very promising for time-dependent problems as well as steady-state entering flows, since the problem of recirculation does not then appear.

Preliminary experiments performed with the advection-diffusion equation are mainly aimed at establishing proper interpolation techniques from the characteristics to the grid. This question is influenced by conservation laws that need to be satisfied and by the order of derivatives which need to be calculated on the grid. Later work will include development of the appropriate DGS scheme and determination of the best location of the pressure variables, which is well suited in the elliptic regime, but may be altered to yield simpler schemes. Such an alteration may benefit the schemes described in this article, too.

Future extension to *compressible flows* is envisioned. For the compressible Euler equations, for example, distribution operators (generalizing (8) above) have been constructed (see, e.g., [2, Section 20.3.2]) which essentially decouple the relaxation process into four sweeps with the advection operator $Q = \mathbf{u} \cdot \partial = u\partial_x + v\partial_y$ (one sweep for each momentum equation, one for the continuity equation and one for the energy equation), and one sweep (a distributive sweep for the equation of state) with the potential-flow operator $L_p = Q^2 - c^2\Delta$, c being the speed of sound. For the sweeps of the advection operator the approaches outlined above can be applied, namely, using downstream relaxation ordering to obtain fast multigrid convergence, and possibly also advecting actually along streamlines, to drastically reduce artificial viscosities. The treatment of the full-potential operator can thus be considered separately. In the case of low Mach numbers $M = |\mathbf{u}|/c$, L_p is uniformly elliptic and the process described in this article is fully applicable. For M approaching 1 and supersonic ($M > 1$) flows, relaxation compatible with the characteristic directions should also be used for L_p. Since L_p has *two* families of characteristic directions, this would generally require *line* relaxation. Fast multigrid convergence with such line relaxation has been demonstrated long ago in [16].

APPENDIX A

The first-order and second-order NUD discretizations for the advection operator $a\partial_x + b\partial_y$ are defined as follows: Let

$$i_1 = i - \operatorname{sgn}(a), \qquad i_2 = i - 2\operatorname{sgn}(a),$$
$$j_1 = j - \operatorname{sgn}(b), \qquad j_2 = j - 2\operatorname{sgn}(b),$$

where the sign function sgn is defined by

$$\operatorname{sgn}(x) = \begin{cases} 1 & x > 0 \\ -1 & x < 0 \\ 0 & \text{otherwise.} \end{cases}$$

Then the first-order approximation to the advection of u in multiplied form is given by

$$h(au_x + bu_y)^h_{i,j} = (|a| - |b|) \cdot (u_{i,j} - u_{i_1,j}) + |b| \cdot (u_{i,j} - u_{i_1,j_1}) \quad (31)$$

if $|a| \geqslant |b|$, and by

$$h(au_x + bu_y)^h_{i,j} = (|b| - |a|) \cdot (u_{i,j} - u_{i,j_1}) + |a| \cdot (u_{i,j} - u_{i_1,j_1}) \quad (32)$$

otherwise. The second-order approximation is given by

$$h(au_x + bu_y)^h_{i,j} = (|a| - |b|) \cdot (1.5u_{i,j} - 2u_{i_1,j} + 0.5u_{i_2,j}) + |b| \cdot (1.5u_{i,j} - 2u_{i_1,j_1} + 0.5u_{i_2,j_2}) \quad (33)$$

if $|a| \geqslant |b|$, and by

$$h(au_x + bu_y)^h_{i,j} = (|b| - |a|) \cdot (1.5u_{i,j} - 2u_{i,j_1} + 0.5u_{i,j_2}) + |a| \cdot (1.5u_{i,j} - 2u_{i_1,j_1} + 0.5u_{i_2,j_2}) \quad (34)$$

otherwise.

The corresponding first-order standard upstream difference scheme (SUD) is given by

$$h(au_x + bu_y)^h_{i,j} = |a| \cdot (u_{i,j} - u_{i_1,j}) + |b| \cdot (u_{i,j} - u_{i,j_1}), \quad (35)$$

and the second-order SUD is given by

$$h(au_x + bu_y)^h_{i,j} = |a| \cdot (1.5u_{i,j} - 2u_{i_1,j} + 0.5u_{i_2,j}) + |b| \cdot (1.5u_{i,j} - 2u_{i,j_1} + 0.5u_{i,j_2}). \quad (36)$$

The local truncation errors τ of the four schemes can be compared by applying them to the solution component $e^{i\omega(ay - bx)}$ of the equation

$$au_x + bu_y = 0,$$

where a and b are constants. Without loss of generality we choose $a \geqslant b > 0$. This yields for the first-order schemes

$$|\tau(\text{SUD})| = \frac{h\omega^2}{2} ab(a+b) + O(h^2\omega^3)$$

$$|\tau(\text{NUD})| = \frac{h\omega^2}{2} ab(a-b) + O(h^2\omega^3),$$

and for the second-order schemes

$$|\tau(\text{SUD})| = \frac{h^2\omega^3}{3} ab(a-b)(a+b) + O(h^3\omega^4)$$

$$|\tau(\text{NUD})| = \frac{h^2\omega^3}{3} ab(a-b)\,|(a-2b)| + O(h^3\omega^4).$$

The leading terms in the local truncation errors of the narrow schemes are seen to vanish at twice as many orientations as those of the corresponding standard schemes. Note that the leading terms in the local truncation errors of the second-order schemes vanish when there is maximal nonalignment of the characteristics with the grid, as well as in the aligned case. In particular, the NUD scheme becomes third-order when $a = 2b$, as noted in Section 4. When a and b are not constant but vary smoothly, these expressions for τ remain the dominant terms in the local truncation errors. This can be seen by transforming the expressions for the local truncation errors of the schemes, obtained from the Taylor series, to a characteristic coordinate system.

The average over the interval $0 \leqslant b \leqslant a$ of the NUD error is smaller than that of the SUD error by a factor of 1:5 in the first-order case, and by a factor of 1:4 in the second-order case.

APPENDIX B

The second-order NUD scheme needs to be modified at $x = h$ for the u advection operator and at $x = h/2$ for the v advection operator, since variables are not defined at points that are at greater distance than h and $h/2$ upstream, respectively. For the advection of u we use

$$u_x(h, y) = 2u_x\left(\frac{h}{2}, y\right) - u_x(0, y) + O(h^2) = 2u_x\left(\frac{h}{2}, y\right) + v_y(0, y) + O(h^2), \quad (37)$$

and

$$u_y(h, y) = u_y(0, y) + hu_{yx}(0, y) + O(h^2) = u_y(0, y) - hv_{yy}(0, y) + O(h^2), \quad (38)$$

where in both equations we have substituted the continuity equation along $x = 0$, and in (38) we have also used the fact that $u_{yx} = u_{xy}$. The terms at the right-hand sides of these equations are approximated by central differences, to yield a second-order upstream scheme.

For the advection of v we use

$$uv_x\left(\frac{h}{2}, y\right) = 2uv_x\left(\frac{h}{4}, y\right) - uv_x(0, y) + O(h^2), \quad (39)$$

where, by the y momentum equation at point $(0, y)$,

$$uv_x(0, y) = -p_y(0, y) - vv_y(0, y). \quad (40)$$

Now

$$p_y(0, y) = p_y\left(\frac{h}{2}, y\right) - 0.5hp_{yx}(0, y) + O(h^2), \quad (41)$$

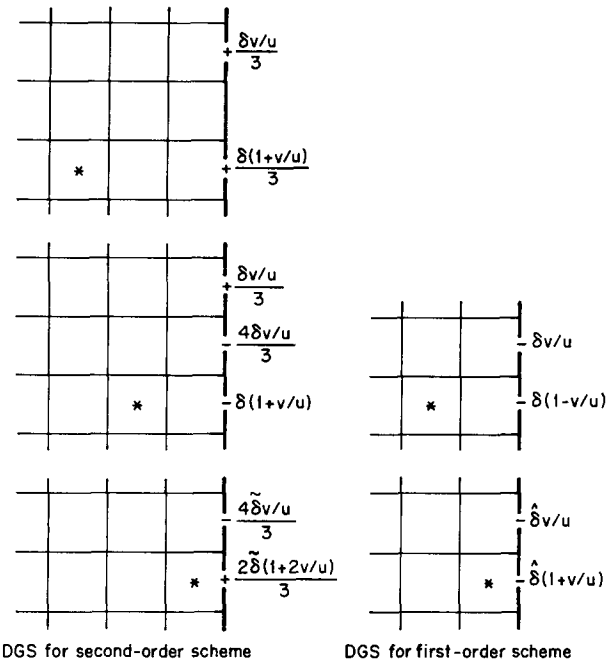

FIG. 3. The changes introduced in the outflow u velocities during DGS relaxation near the outflow boundary are shown. The * marks the cell that is being relaxed. δ, $\tilde{\delta}$, and $\hat{\delta}$ are given by $\delta = hR/4$, $\tilde{\delta} = 3hR/(11 + 4v/u)$, $\hat{\delta} = hR/(4 + v/u)$, where R is the residual of the continuity equation in the relaxed cell before it is relaxed, and v is extrapolated. Otherwise, the DGS relaxation remains as in Fig. 2, except that pressure variables are changed only in the interior of the domain, and, in the cell adjacent to the boundary, δ is replaced by $\tilde{\delta}$ in the second-order scheme and by $\hat{\delta}$ in the first-order scheme.

and $p_{xy}(0, y) = p_{yx}(0, y)$ can be obtained by differentiating the x momentum equation at point $(0, y)$:

$$\begin{aligned} p_{xy}(0, y) &= -(uu_x)_y\,(0, y) - (vu_y)_y\,(0, y) \\ &= uv_{yy}(0, y) - vu_{yy}(0, y), \end{aligned} \tag{42}$$

where we have substituted $-v_y$ for u_x by the continuity equation at point $(0, y)$. Combining Eq. (39)–(42) we obtain

$$\begin{aligned} uv_x\left(\frac{h}{2}, y\right) &= 2uv_x\left(\frac{h}{4}, y\right) + vv_y(0, y) \\ &\quad + 0.5h(vu_{yy} - uv_{yy})(0, y) \\ &\quad + p_y\left(\frac{h}{2}, y\right) + O(h^2). \end{aligned} \tag{43}$$

The right-hand side of Eq. (43) is discretized by central differences, and for the second advection term we used the standard upstream discretization

$$\begin{aligned} hvv_y\left(\frac{h}{2}, y\right) &= v\left(\frac{h}{2}, y\right)\left[1.5v\left(\frac{h}{2}, y\right) - 2v\left(\frac{h}{2}, y - h\right)\right. \\ &\quad \left. + 0.5v\left(\frac{h}{2}, y - 2h\right)\right] + O(h^2), \end{aligned} \tag{44}$$

obtained once again a second-order upstream scheme.

The modifications of the DGS relaxation near the *outflow* boundaries are shown in Fig. 3.

REFERENCES

1. D. Bai and A. Brandt, *SIAM J. Sci. Stat. Comput.* **8**, 109 (1987).
2. A. Brandt, "1984 Multigrid Guide with Applications to Fluid Dynamics," Monograph, GMD-Studie 85, GMD-FIT, Postfach 1240, D-5205, St. Augustin 1, West Germany, 1985 (unpublished). Also available from Secretary, Department of Mathematics, University of Colorado at Denver, Colorado 80204-5300.
3. A. Brandt, "Multigrid Solvers for Non-Elliptic and Singular-Perturbation Steady-State Problems," The Weizmann Institute of Science, Rehovot, Israel, 1981 (unpublished).
4. A. Brandt, "The Weizmann Institute Research in Multilevel Computation: 1988 Report," in *Proceedings of the Fourth Copper Mountain Conference on Multigrid Methods, 1989*, Chap. 2.
5. A. Brandt, "Rigorous Local Mode Analysis of Multigrid," in *Preliminary Proceedings of the Fourth Copper Mountain Conference on Multigrid Methods, 1989.*
6. A. Brandt and N. Dinar, in *Numerical Methods for Partial Differential Equations*, edited by S. Parter (Academic Press, New York/London, 1979), pp. 53.
7. A. Brandt and I. Yavneh, "Accelerated Multigrid Convergence and High-Reynolds Recirculating Flows," LA-UR 90-3368, Los Alamos National Laboratory, Los Alamos, NM. (unpublished).
8. A. Brandt and I. Yavneh, "Efficient Multigrid Solution of the Advection Problem with Closed Characteristics by Upstream Differencing and Downstream Relaxation Ordering," The Weizmann Institute of Science, Rehovot, Israel, 1991 (unpublished).
9. A. Brandt and I. Yavneh, *J. Comput. Phys.* **93** (1), 128 (1991).
10. L. Fuchs and H. S. Zhao, *Int. J. Numer. Methods Fluids* **4**, 539 (1984).
11. W. A. Mulder, *J. Comput. Phys.* **60**, 235 (1985).
12. W. A. Mulder, "Analysis of the Multigrid Method for the Euler Equations of Gas Dynamics in Two Dimensions," in *The Third Copper Mountain Conference on Multigrid Methods, 1987* (unpublished).
13. P. L. Roe and D. Sidilkover, "Optimum Positive Linear Schemes for Advection in Two and Three Dimensions" (unpublished).
14. D. Sidilkover, Ph.D. thesis, The Weizmann Institute of Science, Rehovot, Israel, 1989 (unpublished).
15. D. Sidilkover and A. Brandt, "Multigrid Solution to Steady-State 2D Conservation Laws," in *Preliminary Proceedings of the Fifth Copper Mountain Conference on Multigrid Methods, 1991.*
16. J. C. South and A. Brandt, in *Transonic Flow Problems in Turbomachinery*, edited by T. C. Adamson and M. F. Platzer (Hemisphere, Washington, DC, 1977), p. 180.
17. M. C. Thompson and J. H. Ferziger, *J. Comput. Phys.* **82**, 94 (1989).
18. N. N. Yanenko and Y. I. Shokin, *Dokl. Akad Nauk SSSR* **182**, 776 (1968).